Available on CMS information server

CMS AN 2012/XXX

The Compact Muon Solenoid Experiment

Analysis Note

The content of this note is intended for CMS internal use and distribution only

January 20, 2012

Measurement of the WW Production Cross Section and Limits on Anomalous Couplings

L. Bauerdick, K. Burkett, I. Fisk, Y. Gao, O. Gutsche, B. Hooberman, S. Jindariani, S. Tkaczyk

Fermilab National Accelerator Laboratory, Batavia, USA

G. Bauer, J. Bendavid, E. Butz, M. Chan, V. Dutta, G. Gómez-Ceballos, M. Goncharov, K. Hahn, P. Harris, M. Klute, S. Nahn, C. Paus, D. Ralph, F. Stoeckli, K. Sumorok, K. Sung, R. Wolf, S. Xie, M. Yang, M. Zanetti

Laboratory for Nuclear Science, Massachusetts Institute of Technology, Cambridge, USA

D. Barge, C. Campagnari, D. Kovalskyi, V. Krutelyov

University of California, Santa Barbara, Santa Barbara, USA

W. Andrews, G. Cerati, D. Evans, F. Golf, I. MacNeill, S. Padhi, Y. Tu, F. Würthwein, A. Yagil, J. Yoo

University of California, San Diego, San Diego, USA

I. Kravchenko

University of Nebraska-Lincoln, USA

Abstract

Abstract

Contents

1 Introduction

The W^+W^- diboson production process can be studied to perform accurate tests of the description of electroweak and strong interactions in the Standard Model (SM). Next-to-leading order calculations of W^+W^- production in pp collisions at $\sqrt{s} = 7$ TeV predict a cross-section of $\sigma^{NLO}(pp \to WW \to 2\ell 2\nu) = 43.0 \pm 2.0$ pb [**?**] [25].

Within the SM the dominant W^+W^- production mechanisms are via the s-channel and t-channel diagrams. With the s-channels we can measure WWZ and $WW\gamma$ triple gauge couplings, which are sensitive to possible new physics processes via anomalous couplings. In addition, they represent an important background source for new particle searches, e.g. $H \to W^+W^-$ Higgs boson searches.

This note documents the first W^+W^- production cross-section measurement in 4.63 fb^{-1} of pp collision data at $\sqrt{s} = 7$ TeV using leptonic decays, i.e. $W^+W^- \to \ell^+\nu\ell^-\bar{\nu}$, with electrons and muons in the final state. Fully leptonic tau decays are also considered as a part of the signal, but the selection requirements are not optimized for such events. The work is based on previous studies of W^+W^-[**?**, **?**, **?**] and $H \to W^+W^-$[**?**, **?**] processes performed on simulation.

The note is structured as follows. A brief discussion about the data samples used in the analysis is presented in Sec. 2. Trigger selection, lepton selection, and all kinematic requirements are described in Sec. 3. A summary of the event data yields and the expectations from Monte Carlo is shown in Sec. **??**, followed by the estimation of the backgrounds in Sec. 4. The cross-section measurement, together with all sources of systematic uncertainties are explained in Sec. **??**. Finally, the anomalous couplings limits and conclusions are included in Secs. **??** and 9, respectively.

2 Data Samples

The datasets used for this analysis are summarized in Tables. 1 and 2 for data and Monte Carlo, respectively. The total integrated luminosity is 4.63 fb^{-1}. We used the official good run list [10]. For Monte Carlo simulation we use madgraph when possible, but different generators such as Pythia and Powheg are also used. For $gg \to$ W$^+$W$^-$ a dedicated generator is used. For WZ and ZZ processes we use Pythia, since MadGraph samples are mixed with W$^+$W$^-$ in a single VV sample, which is difficult to use properly.

Dataset Description	Dataset Name
$H \to$ W$^+$W$^-$ Signal Selection Samples	
Run2011A MuEl PromptReco	/MuEG/Run2011A-PromptReco-v*/AOD
Run2011A DiMuon PromptReco	/DoubleMu/Run2011A-PromptReco-v*/AOD
Run2011A SingleMuon PromptReco	/SingleMu/Run2011A-PromptReco-v*/AOD
Run2011A DiElectron PromptReco	/DoubleElectron/Run2011A-PromptReco-v*/AOD
Fake Rate Measurement Samples	
Run2010A Jet PromptReco	/Jet/Run2011A-PromptReco-v*/AOD
Run2010B Photon PromptReco	/Photon/Run2011A-PromptReco-v*/AOD

Table 1: Summary of data datasets used.

3 Event Selection

The fully leptonic final state consists of two isolated leptons and large missing energy from the two undetectable neutrinos. This is the same final state as the non-resonant W$^+$W$^-$ background. The Higgs cross-section is several orders of magnitude lower than the major reducible background processes: $\mathrm{t\bar{t}}$, W+jets and Drell-Yan. We thus perform several steps to select and extract the Higgs boson signal from data:

1. We select events that pass pre-defined lepton triggers.

2. We then select those events with two oppositely charged high p_{T} isolated leptons (ee, $\mu\mu$, $e\mu$) requiring:

With Pileup: Processed dataset name is always /Spring11-PU_S1_START311_V1G1-v*/AODSIM		
Dataset Description	Primary Dataset Name	cross-section (pb)
qq $\rightarrow WW$	/VVJetsTo4L_TuneD6T_7TeV-madgraph-tauola	43.0
gg $\rightarrow WW \rightarrow 2l2\nu$	/GluGluToWWTo4L_TuneZ2_7TeV-gg2ww-pythia6	0.153
$t\bar{t}$	/TTJets_TuneZ2_7TeV-madgraph-tauola	157.5
t(s$-chan$)	/TToBLNu_TuneZ2_s-channel_7TeV-madgraph	1.4
t(t$-chan$)	/TToBLNu_TuneZ2_t-channel_7TeV-madgraph	20.9
tW	/TToBLNu_TuneZ2_tW-channel_7TeV-madgraph	10.6
Z[20-inf] $\rightarrow ee$	/DYToEE_M-20_CT10_TuneZ2_7TeV-powheg-pythia	1666.0
Z[20-inf] $\rightarrow \mu\mu$	/DYToMuMu_M-20_CT10_TuneZ2_7TeV-powheg-pythia	1666.0
Z[20-inf] $\rightarrow \tau\tau$	/DYToTauTau_M-20_CT10_TuneZ2_7TeV-powheg-pythia-tauola	1666.0
Z[10-20] $\rightarrow ee$	/DYToEE_M-10To20_CT10_TuneZ2_7TeV-powheg-pythia	3892.9
Z[10-20] $\rightarrow \mu\mu$	/DYToMuMu_M-10To20_CT10_TuneZ2_7TeV-powheg-pythia	3892.9
Z[10-20] $\rightarrow \tau\tau$	/DYToTauTau_M-10To20_CT10_TuneZ2_7TeV-powheg-pythia-tauola	3892.9
W/Z+γ	/PhotonVJets_7TeV-madgraph	165.0
W $\rightarrow \ell\nu$	/WJetsToLNu_TuneZ2_7TeV-madgraph-tauola	31314.0
WZ	/WZtoAnything_TuneZ2_7TeV-pythia6-tauola	18.2
ZZ	/ZZtoAnything_TuneZ2_7TeV-pythia6-tauola	5.9

Table 2: Summary of Monte Carlo datasets used..

- $p_T > 20$ GeV/c for the leading lepton;
- $p_T > 15/10$ GeV/c for the trailing lepton (same-flavor/opposite flavor);
- standard identification and isolation requirements on both leptons.

3. We apply a common W^+W^- preselection, which requires in brief:
   - categorize events by the number of reconstructed jets;
   - exactly two high p_T isolated leptons;
   - large transverse missing energy due to the neutrinos.
4. Finally, we perform two *Higgs mass dependent* event selections, one cut-based and one using a multivariate technique described in detail in Section **??**.

The W^+W^- preselection steps are now described in detail below.

3.1 Trigger

Triggering on Higgs boson decays in the dilepton final state increases in difficulty with increasing instantaenous luminosity. Single lepton triggers can only be sustained with very tight identification and isolation requirements and large transverse momentum thresholds. This means that double lepton triggers are the only viable option to maintain sensitivity to a low mass Higgs boson, where the leptons transverse momentum can be small.

We designed a suite of signal and control triggers appropriate for this analysis. These dilepton triggers have a high efficiency to collect Higgs boson events and are sufficiently loose to collect control events to estimate fake lepton backgrounds and selection efficiencies with adequate precision. The detailed trigger paths were described in [7].

3.2 Primary Vertex Reconstruction

Primary vertices are reconstructed using the so-called Deterministic Annealing clustering of tracks [13]. Reconstructed primary vertices are required to have a z position within 24 cm of the nominal detector center and a radial position within 2 cm of the beamspot. There must also be greater than four degrees of freedom in the fitted vertex. From the set of primary vertices in the event passing these selection cuts, the vertex with the largest summed squared-p_T of the associated tracks is chosen as the event primary vertex. Reconstructed leptons will be required to have small impact parameters with respect to this vertex.

3.3 Muon Selection

The muon selection is unchanged with respect to [7]. Muons in CMS are reconstructed as either *StandAloneMuons* (track in the muon detector with low momentum resolution), *GlobalMuons* (outside-in approach seeded by a *StandAloneMuon* with a global fit using hits in the muon, silicon strip and pixel detectors) and *TrackerMuons* (inside-out approach seeded by an offline silicon strip track, using the muon detector only for muon identification without refitting the track). Most good quality muons are reconstructed as all three types at the same time and the momentum resolution is dominated by the inner tracker system up to about 200 GeV/c in transverse momentum. We require the muon to be reconstructed as *GlobalMuon*, with χ^2/ndof < 10 on the global fit, must have at least one good muon hit, and at least two matches to muon segments in different muon stations; or *TrackerMuon*, provided it satisfies the "Tracker Muon Last Station Tight" selection requiring at least two muon segments matched at 3σ in local X and Y coordinates, with one being in the outermost muon station.

In addition, the following specific requirements to select good prompt isolated muons are the following:

- more than 10 hits in the inner tracker;
- at least one pixel hit;
- impact parameter in the transverse plane $|d_0| < 0.02$ (0.01) cm for muons with p_T greater (smaller) than 20 GeV/c, calculated with respect to the primary vertex;
- longitudinal impact parameter $|d_z| < 0.1$ cm, calculated with respect to the primary vertex;
- pseudorapidity $|\eta|$ must be smaller than 2.4;
- relative p_T resolution is better than 10%.
- decay in flight with the kink finding algorithm: χ^2/ndof < 20

Furthermore, the particle flow candidate-based isolation variable is used to reduce the contamination from the non-isolated muons originating from jets.

- Iso_PF: defined as the scalar sum of the p_T of the particle flow candidates satisfying the following requirements:
  - $\Delta R < 0.3$ to the muon in the $\eta \times \phi$ plane,
  - $|d_z(\mathrm{PFCandidate}) - d_z(\mathrm{muon})| < 0.1$ cm, if the PF candidate is charged,
  - $p_\mathrm{T} > 1.0$ GeV, if the PF candidate is classified as a neutral hadron or a photon.

We require $\frac{\mathrm{Iso}_\mathrm{PF}}{p_\mathrm{T}} < 0.13$ (0.06) for muons in the barrel with p_T greater (smaller) than 20 GeV/c. For muons in the endcap, we require $\frac{\mathrm{Iso}_\mathrm{PF}}{p_\mathrm{T}} < 0.09$ (0.05) for muons with p_T greater (smaller) than 20 GeV/c.

3.4 Electron Selection

We identify electrons using a multivariate approach optimized for this analysis [12]. In addition, we require some minimal requirements to make sure the electron candidate is as tight as the trigger selection:

- $p_T > 10$ GeV and $|\eta| < 2.5$
- $\sigma_{i\eta i\eta} < 0.01/0.03$ (barrel/endcap)
- $|\Delta\phi_{in}| < 0.15/0.10$
- $|\Delta\eta_{in}| < 0.007/0.009$
- $H/E < 0.12/0.10$ (barrel/endcap)
- $\frac{\sum_\mathrm{trk} E_\mathrm{T}}{p_\mathrm{T}^\mathrm{ele}} < 0.2$

- $\frac{\sum_{\mathrm{ECAL}} E_{\mathrm{T}}}{p_{\mathrm{T}}^{\mathrm{ele}}} < 0.2$
- $\frac{\sum_{\mathrm{HCAL}} E_{\mathrm{T}}}{p_{\mathrm{T}}^{\mathrm{ele}}} < 0.2$

Isolation requirements are then imposed by computing the particle flow isolation, defined as the scalar sum of the p_{T} of the particle flow candidates satisfying the following requirements:

- $\Delta R < 0.4$ to the electron in the $\eta \times \phi$ plane,
- for neutral hadron PF candidates, require that it is outside the footprint veto region of $\Delta R < 0.07$,
- for photon and electron PF candidates, require that it is outside the footprint veto region of $|\Delta\eta| < 0.025$,
- $|d_z(\text{PF candidate}) - d_z(\text{muon})| < 0.1$ cm, if the PF candidate is charged,
- $p_{\mathrm{T}} > 1.0$ GeV, if the PF candidate is classified as a neutral hadron or a photon.

We require $\frac{\mathrm{Iso_{PF}}}{p_{\mathrm{T}}} < 0.13$ (0.09) for electrons in the barrel (endcap).

In order to veto fake electrons from converted photons, we look for a reconstructed conversion vertex where one of the two tracks is compatible with the electron [23]. The vertex fit probability is required to be $> 10^{-6}$. We then require that there are no missing expected missing hits forming the electron track [23], [14]. Finally to reduce fake electrons from non-prompt sources, we require the transverse and longitudinal impact parameters with respect to the primary vertex to be less than 0.02 and 0.1 cm respectively.

3.5 Missing Energy

The missing transverse energy is used to reject background events where there is no natural source of missing energy, like in Drell-Yan and QCD events. In the $Z/\gamma^* \to \tau\tau$ process there is a large difference in the masses of τ and Z. The taus are produced with large boost and their decay products, including neutrinos, are aligned with the leptons. Therefore a transverse component of missing energy with respect to the leptons is a better measure of true missing energy in the event, not originating from τ decay. To reject such background events with a small opening angle between $E_{\mathrm{T}}^{\mathrm{miss}}$ and one of the leptons, we used the projected $E_{\mathrm{T}}^{\mathrm{miss}}$ [7] for event selection, defined as:

$$\text{with } \Delta\phi_{min} = min(\Delta\phi(\ell_1, E_{\mathrm{T}}^{\mathrm{miss}}), \Delta\phi(\ell_2, E_{\mathrm{T}}^{\mathrm{miss}})) \tag{1}$$

$$= \begin{cases} E_{\mathrm{T}}^{\mathrm{miss}} & \text{if } \Delta\phi_{min} > \frac{\pi}{2}, \\ E_{\mathrm{T}}^{\mathrm{miss}} \sin(\Delta\phi_{min}) & \text{if } \Delta\phi_{min} < \frac{\pi}{2} \end{cases} \tag{2}$$

where $\Delta\phi(\ell_i, E_{\mathrm{T}}^{\mathrm{miss}})$ is the angle between $E_{\mathrm{T}}^{\mathrm{miss}}$ and lepton i in the transverse plane. In the presence of high multiple-interactions (pile-up), the instrumental $E_{\mathrm{T}}^{\mathrm{miss}}$ tail in $Z/\gamma^* \to \ell\ell$ events increases significantly.

To improve the signal over background performance of $E_{\mathrm{T}}^{\mathrm{miss}}$ selections in the presence of pile-up, we have developed a novel $E_{\mathrm{T}}^{\mathrm{miss}}$ algorithm referred to as "trk-MET" [36], constructed from charged particles consistent with originating from the primary vertex. The event $E_{\mathrm{T}}^{\mathrm{miss}}$ trk-MET is defined as

$$\text{trk-MET} \equiv -\overrightarrow{p_T}(l_1) - \overrightarrow{p_T}(l_2) - \sum_i \overrightarrow{p_T}(i), \tag{3}$$

where $\overrightarrow{p_T}(l_1)$ and $\overrightarrow{p_T}(l_2)$ are the transverse momentum vectors of the two leptons passing the lepton selections described in Section 3.3 and Section 3.4, and $\overrightarrow{p_T}(i)$ represent the tranverse momentum vectors of the charged PFCandidates satisfying the following requirements:

- the track matched to PFCandidate has $\Delta z < 0.1$ cm with respect to the signal primary vertex;
- the track has $\Delta R > 0.1$ with respect to both leptons, to avoid double-counting of the leptons.

Comparing to the projected PFMet, we observed that the projected trk-MET has a larger tail in $Z/\gamma^* \to \ell\ell$ background events [36]. However these two $E_{\mathrm{T}}^{\mathrm{miss}}$ values are weakly-correlated in $Z/\gamma^* \to \ell\ell$ backgrounds with no geninue $E_{\mathrm{T}}^{\mathrm{miss}}$, and strongly correlated for the signal processes with geninue $E_{\mathrm{T}}^{\mathrm{miss}}$. Therefore the signal over background ratio is improved if we select the events based on the mininum of these two projected $E_{\mathrm{T}}^{\mathrm{miss}}$ values, min-MET $\equiv min(\mathrm{proj}_{\text{trk-MET}}, \mathrm{proj}_{\mathrm{PFMET}})$.

The selection requirements are different between $ee/\mu\mu$ and $e\mu$ final states since Drell-Yan mostly contributes to ee and $\mu\mu$ channels. The selection requirements are:

- min-MET > 20 GeV for $e\mu$;
- min-MET $> (37 + N_{vtx}/2)$ GeV for ee and $\mu\mu$.

3.6 Z Veto

To further reduce the Drell–Yan background in the $\mathrm{e}^+\mathrm{e}^-$ and $\mu^+\mu^-$ final states, we veto events with a dilepton invariant mass within 15 GeV of the Z. We also reject events with a dilepton invariant mass below 20 GeV (same-flavor) and 12 GeV (opposite flavor) to suppress contributions from low mass resonances as well as to reject low mass Drell–Yan contribution that is poorly simulated at the moment.

3.7 Jet Veto

Jets are reconstructed using calorimeter and tracker information using a particle flow algorithm [20]. The anti-$\mathrm{k_T}$ clustering algorithm [22] with R = 0.5 is used. We apply the standard jet energy corrections [19] to the reconstructed jets, where the L1 Fast Jets corrections are included. The latter corrections are rather important since they help in flatening the reconstruction efficiency as a function of the number of overlapping events. To exclude electrons and muons from the jet sample, these jets are required to be separated from the selected leptons in ΔR by at least $\Delta R^{\mathrm{jet-lepton}} > 0.3$.

In this analysis we use high p_T jets to define the analysis jet bin and low p_T jets to do the top events veto. We define:

- *counted jet*: a reconstructed jets with $p_{\mathrm{T}} >$ 30 GeV within $|\eta| < 5.0$;
- *low p_T jet*: a reconstructed jets with 10 $< p_{\mathrm{T}} <$ 30 GeV within $|\eta| < 5.0$

We analyze the events separately based on the number of counted jets in the event.

3.8 Top Tagging

Because the production cross-section is substantially higher than the $\mathrm{W^+W^-}$ cross-section, top backgrounds pose a significant challenge. To reduce the top background, we introduce two top tagging methods. Both methods rely on the fact that top quarks decay to Wb with almost certainty.

The first method vetoes events containing soft muons from the b-quark decays. The requirements used to select soft muons are:

- $p_{\mathrm{T}} > 3$ GeV;
- Reconstructed as a TrackerMuon
- Meets TMLastStationAngTight muon id requirements
- The number of valid inner tracker hits > 10
- The transverse impact parameter with respect to the Primary Vertex, $|d_0| < 0.2$ cm,
- The longitudinal impact parameter with respect to the Primary Vertex $|d_z| < 0.2$ cm. This requirement has been loosened with respect to [7];
- Non-isolated ($\mathrm{Iso_{Total}}/p_{\mathrm{T}} > 0.1$) if $p_{\mathrm{T}} > 20$GeV.

The second method uses standard b-jet tagging [7]. In this method, events containing jets tagged with the TrkCountingHighEff [21] algorithm with a discriminator value of greater than 2.1 are vetoed. The algorithm is applied to jets with the same definition as Section 3.7, with the exception that we consider jets with $E_{\mathrm{T}} > 10$ GeV, and we require $\frac{|\sum^{i} d_{z}^{i}(p_{\mathrm{T}}^{i})^{2}|}{\sum^{i} (p_{\mathrm{T}}^{i})^{2}} < 2$, where the sum runs over all tracks that belongs to each jet. These two requirements are different with respect to [7], with the effect of reducing the mistag rate and the dependency on pile-up. By using the expected tagging efficiency for the two methods, it is possible to estimate the residual top background after the vetoes have been applied. This is described in detail in Section 4.2.

3.9 Other Preselection Requirements

To reduce the background from diboson processes, we veto events containing an additional lepton meeting the previously described selection requirements with $p_{\mathrm{T}} > 10$ GeV/c. This removes $\sim 60\%$ of the WZ component and $\sim 10\%$ of the ZZ one. The ZZ component is dominated by ZZ $\rightarrow 2l2\nu$ decays. The efficiency for $WW \rightarrow 2l2\nu$ events is $\sim 99.9\%$. Finally, the angle in the transverse plane between the dilepton system and the most energetic jet with $p_{\mathrm{T}}^{jet} > 15$ GeV must be smaller than 165 degrees in the $ee/\mu\mu$ final states. This requirements rejects $Z/\gamma^{*} \rightarrow \ell\ell$ events, where the Z boson recoil against a jet.

4 Background Estimation

4.1 Jet Induced Backgrounds

Jet induced fake leptons are an important source of background for many physics channels. In this analysis the main sources of fake leptons are W + jets and QCD events, where at least one of the jets or a constituent is misidentified as an isolated lepton. The dominant background is W + jets because there is already one prompt, well isolated, lepton from the W boson decay. Fake non-prompt leptons arise from the leptonic decay of heavy quarks, misidentified hadrons or electrons from photon conversion.

A data-driven approach, described in detail in [15] and [16], is pursued to estimate this background. Only a summary of the method is described here, more details can be found in [7]. A set of loosely selected lepton-like objects, referred to as the "fakeable object" or "denominator" from here on, is defined in a sample of events dominated by dijet production. The efficiency for these denominator objects to pass the full lepton selection critera is measured. This background efficiency, typically referred to as the "fake rate", is parameterized as a function of the p_{T} and η of the denominator object in order to capture any dependence on kinematic and geometric quantities. We will denote the fake rate symbollically by ϵ_{fake}. These fake rates are, then, used as weights to extrapolate the background yield from a sample of loose denominator objects to the sample of fully selected leptons.

4.1.1 Denominator Object Definitions

The denominator object definition has significant impact on the systematic uncertainty of the method, due to the fact that the sample dependence uncertainties for extrapolating in different isolation and lepton quality criteria are typically different. We consider the following definition:

- $\sigma_{i\eta i\eta} < 0.01/0.03$ (barrel/endcap)
- $|\Delta\phi_{in}| < 0.15/0.10$
- $|\Delta\eta_{in}| < 0.007/0.009$
- $H/E < 0.12/0.10$
- full conversion rejection
- $|d_0| < 0.02$ cm
- $\frac{\sum_{\mathrm{trk}} E_{\mathrm{T}}}{p_{\mathrm{T}}^{\mathrm{ele}}} < 0.2$
- $\frac{\sum_{\mathrm{ECAL}} E_{\mathrm{T}}}{p_{\mathrm{T}}^{\mathrm{ele}}} < 0.2$
- $\frac{\sum_{\mathrm{HCAL}} E_{\mathrm{T}}}{p_{\mathrm{T}}^{\mathrm{ele}}} < 0.2$

The situation for muons is simpler. The loose muon selection requirements can differ from the tight selection of Section 3.3, only in less stringent cuts on d_0 and isolation. We consider the following definition:

- $|d_0| < 0.2$ cm
- $\frac{\mathrm{Iso}_{\mathrm{Total}}}{p_{\mathrm{T}}} < 0.4$

4.1.2 Fake rate measurement

The fake rates are measured in calibration data samples dominated by fake leptons resulting from jets in QCD dijet events. The QCD dijet event sample is collected using a combination of different electron and muon triggers.

In order to suppress contamination due to signal leptons from the decay of W and Z bosons we require that the missing transverse energy is less than 20 GeV, and that the event contains only a single reconstructed lepton. In order to control the average p_T of the jet that fakes the lepton, we impose a p_T requirement on the leading jet in the event and require that the lepton denominator object is separated from the leading jet by ΔR > 1.0. The nominal fake rates for electrons are measured requiring that the leading jet p_T is greater than 35 GeV, and the nominal fake rates for muons are measured with the requirement that the leading jet p_T is greater than 15 GeV. From these selected event samples, we measure the fake rate (ϵ_{fake}) by counting the number of denominator objects which pass the full lepton selection, in bins of p_T and η.

4.1.3 Application of Fake rates

Having measured the fake rates, parameterized in the kinematic quantities of interest, we then use them as weights in order to extrapolate the yield of the sample of loose leptons to the sample of fully selected leptons. This is done by selecting events passing the full event selection described in Sec.3, with the exception that one of the two lepton candidates is required to pass the denominator selection cuts but fail the full lepton selection cuts. This lepton is from here on denoted the "failing leg". The other lepton is required to pass the full selection. The data sample selected in this way is denoted the "tight + fail" sample. Each of the events passing this selection is given a weight computed from the fake rate in the particular p_T and η bin of the failing leg, as follows:

$$w_i = \frac{\epsilon_{\text{fake}}(p_{\text{Ti}}, \eta_i)}{1 - \epsilon_{\text{fake}}(p_{\text{Ti}}, \eta_i)} \tag{4}$$

where i is an index denoting the failing leg, and p_{Ti} and η_i are the transverse momentum and pseudorapidity of the failing leg. Summing the weights w_i over all such events in the tight + fail sample yields the total jet induced background prediction.

This tight + fail extrapolation prediction will in fact double count the QCD component of the background, where both leptons are jet induced fakes. This is essentially a combinatorial artifact, due to the fact that in the tight plus fail selection, one is unable to uniquely distinguish which lepton is required to be the tight one and which lepton is required to be the failing one, and therefore one customarily selects both combinations. This double fake background is typically very small and accounts for roughly a few percent of the total jet induced background. In order to estimate the amount of double counting, we perform the fake rate extrapolation on both lepton legs, selecting events which pass all event selection criteria, except that both leptons are required to pass the denominator selection, but fail the full lepton selection. This event sample is denoted as the "fail + fail" sample. Events in the fail + fail sample are then given weights as follows:

$$w_{i,j} = \frac{\epsilon_{\text{fake}}(p_{\text{Ti}}, \eta_{\text{i}})}{1 - \epsilon_{\text{fake}}(p_{\text{Ti}}, \eta_{\text{i}})} \times \frac{\epsilon_{\text{fake}}(p_{\text{Tj}}, \eta_{\text{j}})}{1 - \epsilon_{\text{fake}}(p_{\text{Tj}}, \eta_{\text{j}})} \tag{5}$$

where i and j denote the two failing leg, and $p_{\text{Ti/j}}$ and $\eta_{\text{i/j}}$ are the transverse momentum and pseudorapidity of the first and second leg. Summing the weights $w_{i,j}$ over all such events in the fail + fail sample yields the total QCD double fake background. This prediction is then subtracted from the tight + loose prediction in order to account for the double counting.

In this procedure, an over-estimation of the fake lepton contribution due to contamination from real dilepton events, and from $W + \gamma$ events may occur. These contributions are subtracted using the Monte Carlo simulation prediction with the procedure described in [15] and [17].

4.2 Top Background

The top quark induced background in the W^+W^- analysis originates from $\text{t}\bar{\text{t}}$ and the single top (tW) processes, the latter being especially imporatant in the 0-Jet bin. A consistent theoretical description of the two processes at high perturbation orders is not straightforward to attain as already at NLO some tW diagrams coincides with LO $\text{t}\bar{\text{t}}$ ones [42]. The Monte Carlo simulated samples used in the analysis exploit an approach recently proposed [43], which addresses the overlap by discarding the common diagrams from the tW process either at amplitude level (*Diagram Removal*) or at cross section level (*Diagram Subtraction*). The former is considered the default scheme, whereas the latter is used as cross check.

The procedure to estimate the top background from data in the case of the 0-Jet bin established in [7] has been adapted to the new theoretical description of $\mathrm{t\bar{t}}$ and tW. Before assessing the adjustments to the procedure, it is worth reviewing the key points of the normalization strategy.

Rejection for the top background is achieved by top-tagged events, i.e. events with a b-tagged jet or a soft muon as defined in Section 3.8. The estimation of this background relies on the measurement on data of the top-tagging efficiency. The procedure deployed in [7] in the case of the 0-Jet bin proceeds accordingly to the following steps:

1. A top enriched region is defined requiring exactly one b-tagged jet with p_{T}larger than 30 GeV (denumerator). Those events among this sample with at least one b-tagged jets with $10 < p_{\mathrm{T}} < 30$ GeV or one soft muon defines the numerator. The ratio of the yields in the numerator and denumerator properly corrected from other backgrounds contamination provides the top-tagging efficiency for one "top-taggable" leg, ϵ_{1leg}^{data}.

2. The actual top-tagging efficiency, ϵ_{topTag}^{data}, is computed accounting for the $\mathrm{t\bar{t}}$fraction of the top background ($f_{t\bar{t}}^{MC}$) accordingly to the formula:

$$\epsilon_{topTag}^{data} = f_{t\bar{t}}^{MC}(1-(1-\epsilon_{1leg}^{data})^2) + (1-f_{t\bar{t}}^{MC})\epsilon_{1leg}^{data} \tag{6}$$

   where the first term on the right accounts for $\mathrm{t\bar{t}}$ (two taggable legs) and the second term for tW (one taggable leg). The value $f_{t\bar{t}}^{MC}$ is determined from Monte Carlo in the 0-Jet bin at the $\mathrm{W^+W^-}$ preselection level, removing the anti top-tagging.

3. A dedicated control region is defined in the 0-Jet bin by requiring top-tagged events. The data yields in this region corrected for the other backgrounds contaminations are then used together with top-tagging efficiency to predict the top background after $\mathrm{W^+W^-}$ preselections level:

$$N_{WWregion}^{top} = N_{topTag}^{top}\frac{1-\epsilon_{topTag}^{data}}{\epsilon_{topTag}^{data}} = (N_{topTag}^{data} - N_{other-bkg}^{data})\frac{1-\epsilon_{topTag}^{data}}{\epsilon_{topTag}^{data}} \tag{7}$$

The top background is estimated at the $\mathrm{W^+W^-}$ preselections level where a common scale factor for the Monte Carlo $\mathrm{t\bar{t}}$ and tW samples is computed. Once properly normalized, those samples are used either to predict the correspoding yields after the mass dependent Higgs selections for the cut based analysis (Section **??**), or as templates for the multivariate analysis.

In a nutshell, the new procedure refines the way the top-tagging efficiency is extracted from data, taking properly into account the different features of $\mathrm{t\bar{t}}$ and tW.

- The top-tagging efficiency for one leg, ϵ_{1leg}^{data}, is computed for $\mathrm{t\bar{t}}$ only, that is both non-top backgrounds and tW yields are subtracted from the measured data in the 1-Jet bin control region defined above (both numerator and deniminator). The yields for tW are estimated from the Monte Carlo normalized accordingly to the data-driven predictions in the 1-Jet bin previously evaluated.

- The overall top-tagging efficiency, ϵ_{topTag}^{data}, is then redefined to account for the fraction of tW events that looks like $\mathrm{t\bar{t}}$ (x), that is with two top-taggable legs. Equation 6 thus becomes:

$$\epsilon_{topTag}^{data} = (f_{t\bar{t}}^{MC} + x(1-f_{t\bar{t}}^{MC}))(1-(1-\epsilon_{1leg}^{data})^2) + (1-f_{t\bar{t}}^{MC})(1-x)\epsilon_{1leg}^{data} \tag{8}$$

  The fraction x matches the value of ϵ_{1leg} estimated from the tW Monte Carlo. We consider this a good approximation as ϵ_{1leg} is the fraction of events with one b-tagged jet with p_{T}larger than 30 GeV (the first "top-taggable" leg) and top-tagged leg (a b-tagged jets below 30 GeV or a soft muon).

The extrapolation from the top background control region in the 0-Jet bin to the signal $\mathrm{W^+W^-}$ region is still performed accordingly to Equation 7, where ϵ_{topTag}^{data} is now defined by Eq. 8.

The plots in Figure 1 show the distribution of the b-tag discrimiator for the jet with p_{T} lower than 30 GeV and the highest b-tag discriminator in the 1-Jet (denumerator and numerator) and 0-Jet bins control region.

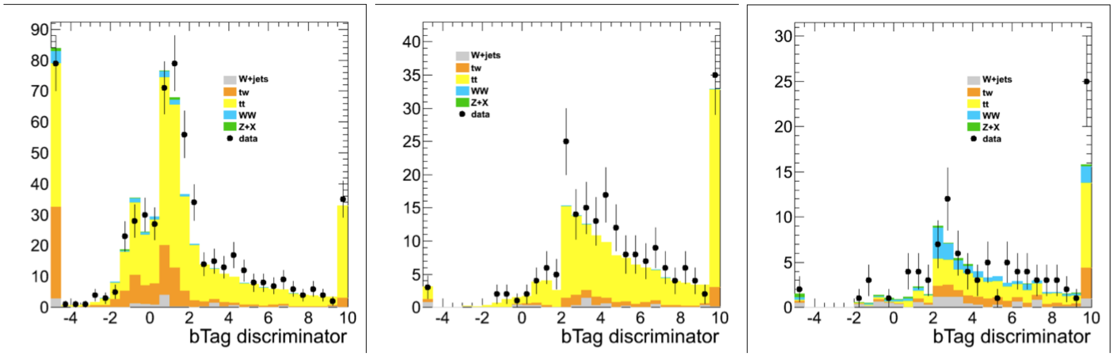

Figure 1: b-tag discrimiator distribution for the jet with $p_T < 30$ GeV and the highest b-tag discriminator in the 1-Jet (denumerator, left and numerator, center) and 0-Jet bins control region (right).

4.3 Drell-Yan Background

We apply a data-driven method [18] to estimate the $Z/\gamma^* \to \ell\ell$ contributions in the same flavor $\ell^+\ell^-$ final states. The expected contributions from $Z/\gamma^* \to \ell\ell$ events outside the Z-mass region in data can be estimated by counting the number of events near the Z mass region in data, subtracting from it the non-Z contributions, and scaling it by a ratio $R_{out/in}$ defined as the fraction of events outside and inside the Z-mass region in the simulation. The Z-mass region is selected to be within 7.5 GeV of the nominal Z mass. The tight window is chosen to reduce the non-Z contributions from top and multi-boson backgrounds. The non-Z contributions close to the Z-mass region in data is estimated from the number of events in the $e^{\pm}\mu^{\mp}$ final state $N_{in}^{e\mu}$, applying a correction factor that normalizes the electron-to-muon efficiency $k_{ee/\mu\mu}$. $R_{out/in}$ can be obtained both from simulation and data. In simulation it is defined as the ratio N_{out}^{MC}/N_{in}^{MC}.

This method is described mathematically as:

$$N_{out}^{ll,exp} = R_{out/in}^{ll}(N_{in}^{ll} - 0.5 N_{in}^{e\mu} k_{ll}), \tag{9}$$

where $k_{ee} = \sqrt{\frac{N_{in}^{ee,loose}}{N_{in}^{\mu\mu,loose}}}$ for $Z/\gamma^* \to ee$ and $k_{mm} = \sqrt{\frac{N_{in}^{\mu\mu,loose}}{N_{in}^{ee,loose}}}$ for $Z/\gamma^* \to \mu\mu$. In the k_{ll} calcualtion, we apply a loose $E_{\mathrm{T}}^{\mathrm{miss}}$ cut on minMET of 20 GeV.

The ZZ/ZW processes contribute to the events in the control region of the $m_{\ell\ell}$ region dominated by the DY. The contribution from ZZ/ZW becomes comparable to the Drell-Yan background after a tight projected $E_{\mathrm{T}}^{\mathrm{miss}}$selection in the same flavor final states. The ZZ/ZW events contain natural $E_{\mathrm{T}}^{\mathrm{miss}}$, for which the detector simulation is reliable[1)]. We subtract the expected peaking ZZ/ZW contribution to the yield in the Z peak using the simulation in the estimation of number of events within the Z window in data:

$$N(\ell\ell)_{\mathrm{signal}}^{\mathrm{DY}} = (N(\ell\ell)_{\mathrm{control}}^{\mathrm{data}} - 0.5 \times N(e\mu)_{\mathrm{control}}^{\mathrm{data}} \times k_{\ell\ell} - N_{\mathrm{control}}^{\mathrm{ZV,\ sim.}}) \times R(\ell\ell)_{out/in}^{DY} \tag{10}$$

The ZZ/ZW contribution in the same flavor final states is then taken directly from simulation. Seperating the Drell-Yan and ZZ/WZ components accounts for the fact that the extrapolation from control region to signal region can be different for the two processes when considering the full Higgs selection. We assume an overall 10% uncertainty on the ZZ/ZW yield in the peak, which is anyway overshadowed by the statistical uncertainty on the observed events in the Z peak in data.

This $Z/\gamma^* \to \ell\ell$ estimation method relies on the assumption that the dependence of the ratio $R_{out/in}$ on the $E_{\mathrm{T}}^{\mathrm{miss}}$ cut is well modelled by simulation and is relatively flat. The variations in the $R_{out/in}$ in different $E_{\mathrm{T}}^{\mathrm{miss}}$ regions are assigned as systematics. The $E_{\mathrm{T}}^{\mathrm{miss}}$ regions considered are [20, 25], [25-30], [30-37] and [37, above]. As we do not see any statistically difference between the ee and $\mu\mu$ final states, we combine the two final states to gain statistical stability.

1) The ZZ/ZW events with no $E_{\mathrm{T}}^{\mathrm{miss}}$are suppressed by the same large factor as the DY ones, and therefore their contribution is as negligible at the level of the final selection as it would be in the yield at the Z peak without $E_{\mathrm{T}}^{\mathrm{miss}}$requirement.

N_{in}(data)	$R_{out/in}$	N_{out}(data)	N_{out}(MC)	SF(Data/MC)
89.52 ± 21.33	0.11 ± 0.02 ± 0.14	10.13 ± 2.91 ± 12.34	4.18 ± 1.13	2.43 ± 3.03

Table 3: The Drell-Yan estimation in the same flavor final state.

We cross-checked the $R_{out/in}$ value in data as well. Background processes contribute equally to ee, $e\mu$, μe and $\mu\mu$ final states (after efficiency corrections), while Drell-Yan only contributes to ee and $\mu\mu$. Therefore we can subtract $e\mu$ and μe contribtutions from ee and $\mu\mu$ ones to get an estimate of Drell-Yan. We have found good agreement between data and MC in the Drell-Yan dominated regions, shown in Figure 2.

Table 3 shows the estimation of the Drell-Yan background.

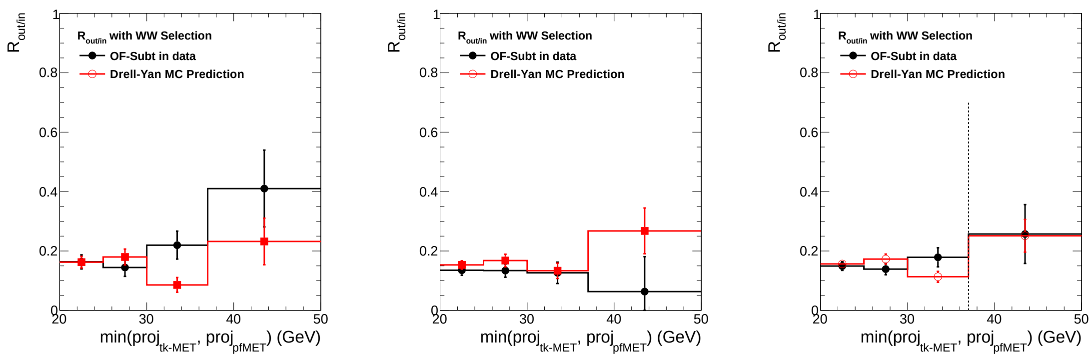

(a) ee (b) mm (c) ee/mm combined

Figure 2: The $R_{out/in}$ as a function of MET measured from data (black solid dots) and MC (red open circles) for the Drell-Yan processes. The measurements in data are done using the opposite flavor subtraction method.

4.4 Other Backgrounds

There are three processes which need to be estimated from Monte Carlo simulation, after applying the proper data corrections for lepton, trigger and jet veto efficiencies, in this low luminosity regime: WZ, ZZ, and $W + \gamma$.

WZ and ZZ events with lepton pairs from a resonant Z boson are suppressed by the Z veto. The remaining contribution is expected to be well modeled in the simulation and thus the Monte Carlo prediction is used.

The $W + \gamma$ background, where the γ fakes an electron through an asymmetric conversion is difficult to estimate from data. Additional cross-checks can be performed to place data based constraints on this estimate. For instance, applying the same standard selection, but requiring two same-sign leptons, gives a sample dominated by W + jets and $W + \gamma$ events. Again, the expected contribution is very small, due to stringent γ conversion requirements explained in Sec. 3.4.

5 Efficiency Measurements

5.1 Lepton Efficiency

We used the tag and probe method on $Z/\gamma^* \rightarrow \ell\ell$ events to provide an unbiased, high-purity, lepton sample with which to measure both online and offline selection efficiencies. This method, which is now described, has been used successfully in previous CMS analyses [31][32].

5.1.1 Method

For muons, we used the lowest threshold unprescaled single muon triggered sample from the Prompt Reco. For electrons we used events triggered by the dedicated double electron tag and probe trigger, where tight electron requirements are imposed on one leg and the other leg is a super cluster.

At least one of the leptons, the *tag*, was required to pass the full selection criteria while the other lepton, the *probe*, was required to pass a set of identification criteria leaving it unbiased with respect to the criterion under study. By requiring that the tag was able to have passed the single lepton trigger on which the events were acquired, we reduced the bias due to the trigger on the probe. Also, the tight criteria imposed on the tag coupled with the invariant mass requirement improves the purity of the sample. Because the analysis uses the same mass window to reduce the $Z/\gamma^* \to \ell\ell$ contribution, the tag and probe sample represents an independent control sample.

To extract the efficiency of the offline selection and the trigger on a per lepton basis, we used two independently developed implementations of the method. The first implementation counts tag-probe pairs, thus an event that contains two leptons meeting the tag criteria could be counted twice. The efficiency is then $\varepsilon = TP/(TP + TF)$, where TP is the number of probes that pass the criteria under study and TF is the number that fail. To estimate and subtract any residual background contribution a simultaneous fit was performed to the TP and TF mass distributions in the range $50 < M_{ll} < 130$. The signal model was taken from simulation, with a gaussian smearing component to take into account the resolution. The background model is an exponential. This method and its associated systematics are discussed in detail in Reference [31]

The second implementation counts events rather than tag-probe pairs. This method is discussed in detail in Reference [32]. In this case the events are divided into three categories,

- 2TT: Both leptons passed the tight criteria, including the trigger. This means that either lepton could be used as a probe, so such events were counted twice.
- TP: The probe passed the selection criterion but did not pass the tight criteria.
- TF: The probe failed the selection criterion.

The efficiency in terms of the categories is $\varepsilon = \frac{2TT+TP}{2TT+TP+TF}$. If criteria tested on the probe are a subset of the tag criteria then this method is equivalent to counting tag-probe pairs because an event with two tags would be counted twice in both methods. The efficiency was extracted by counting the number of events in each category. To reduce any residual background this was done by factorising the selection in N steps and then measuring the efficiency of each step with respect to the others. This is referred to as the N-1 method. The bias on the efficiency from changing the denominator is assessed using simulation and propaged to the uncertainty on the efficiency extracted. If the bias is small or the scale factor is close to unity then the bias on the scale factor is very small.

The offline selection results shown here use the N-1 method with simple counting. We split the results into the detector regions $|\eta| < 1.479$ and $1.479 < |\eta| < 2.50$ to reflect the divisions that define our event selections. In each η bin we measured the scale factor between data and simulation for $10 \leq p_T < 15$, $15 \leq p_T < 20$ and $p_T \geq 20$. The trigger selection results are shown in the minimum number of bins required to capture the efficiency below the kinematic turn-on, in the region of the turn-on and at plateau.

To produce overall data-MC scale factors to apply in the analysis, we factorise the efficiency measurements into two steps such that

$$\varepsilon_{total} = \varepsilon_{offline} \times \varepsilon_{trigger}. \tag{11}$$

The offline efficiency $\varepsilon_{offline} = \varepsilon^{l1}_{offline} \times \varepsilon^{l2}_{offline}$ is the product of the efficiencies of the two leptons and is discussed in more detail in Sections 5.1.2 and 5.1.3 for electrons and muons respectively. The trigger efficiency is measured with respect to the offline selection and is discussed in more detail in Section 5.1.4.

5.1.2 Electron Efficiency

The electron selection efficiency can be factorised into two contributions, the efficiency from the electron reconstruction and from the additional analysis selections that are described in Section 3.4.

The electron reconstruction efficiency is defined as the efficiency for a supercluster to be matched to a reconstructed ECAL driven GSF electron. The data to simulation scale factor was measure by the

Egamma POG binned in p_T and η [33]. From these studies, we take an overall scale factor of 0.99 with an uncertainty of 2.0%.

We thus measure the efficiency of our offline analysis selection with respect to a reconstructed ECAL driven GSF electron denominator. The efficiency measurement results are tabulated in detail in Appendix **??**. For electrons with p_T above 20 GeV the efficiency is roughly 80% for the barrel and 65% for the endcap, while for electrons with p_T below 20 GeV the efficiency is about 40% for the barrel and 20% for the endcap.

The Monte Carlo to data scale factors for the electron selection efficiency are on average near 1 for all electrons except endcap electrons with p_T below 20 GeV for which the scale factor is roughly 1.1. There is a significant decrease from the Run2011A period to the Run2011B period in signal efficiency for electrons with p_T below 20 GeVdue to the effect of pileup on the isolation requirement. A corresponding but smaller decrease in the Monte Carlo to data scale factor is observed.

5.1.3 Muon Efficiency

The muon selection efficiency and the resulting data to simulation scale factors are estimated using a similar method to the electron efficiency. The efficiency for reconstructing a global muon or a tracker muon with respect to a track is measured to be consistent with 100% for the Run2011A period, while it is roughly 99% in the region of the detector covered by the CSC muon detectors in the Run2011B period, summarized in Table **??**.

We measure the offline muon selection efficiency with respect to a reconstructed global muon or tracker muon denominator. The muon selection efficiency measurement results are tabulated in detail in Appendix **??**. The Monte Carlo to data scale factors for the muon selection efficiency are on average around 0.97 for p_T below 20 GeV and 0.99 for p_T above 20 GeV. Analogous to electrons, there is a decrease in signal muon efficiency of $7 - 8\%$ from the Run2011A period to the Run2011B period for muons with p_T below 20 GeV, and a corresponding but smaller decrease in the Monte Carlo to data scale factor.

5.1.4 Trigger Efficiency

To determine the efficiency of the dilepton triggers, we derive the efficiency of the requirements imposed on each leg separately. This requires a modification to the tag and probe method described above in some cases. If the trigger objects are saved by the HLT before the requirement that there be two valid objects then we can check each leg independently of the other using the usual tag and probe method. If the trigger objects are saved after the requirement that there are two valid objects, then there is a 100% correlation between the decision we can probe on each lepton. This means that we must pick exactly one tag candidate for each event a priori, which we do randomly. If the randomly selected tag candidate meets the tight requirements then we are free to probe the other lepton.

The double electron trigger requires the higher p_T leg to be seeded at Level-1. The efficiency of the seeded leading leg with respect to an electron passing offline selection is tabulated in Table **??** of Appendix **??**. The efficiency for the trailing unseeded leg is given in Table **??**. The efficiency of the single electron trigger with respect to an electron passing offline selection is given in Table **??**. The listed values represent the overall efficiencies averaged over the run range of the dataset, absorbing changes in thresholds and seeding requirements over time.

The efficiency of the leading and trailing legs of the double muon trigger is summarized in Tables **??** and **??**. The efficiency of the single muon trigger is given in Table **??**.

In the case of the $e\mu$ triggers, we cross check the trigger efficiency against the leading and trailing legs of the double electron and double muon triggers using dilepton $t\bar{t}$ events requiring that the event has missing transverse energy greater than 20 GeV. The efficiency of the muon leg are measured using events passing the single electron trigger, while the efficiency of the electron leg are measured using events passing the single muon trigger. They are found to be consistent within statistical uncertainties. We thus take the single leg efficiencies from the double electron and double muon triggers for the cross triggers as well.

Having measured the per lepton trigger efficiencies and for the double and single trigger, we compute the efficiency for dilepton events to be selected. We do this by taking into account the two ways an event can be selected: the double trigger can pass or the double trigger can fail because one leg is bad but the good leg can pass the single trigger. If both legs are bad in the double trigger they will also both be bad in the single trigger because the requirements of the single trigger are tighter than any single leg of the double trigger. Thus taking into account combinatorics, the event efficiency $\varepsilon_{\ell\ell'}(p_T,\, \eta,\, p'_T,\, \eta')$ is given in Equation 12, where $\varepsilon_S(p_T,\, \eta)$ is the single lepton trigger efficiency, $\varepsilon_{\mathrm{D,leading}}(p_T,\, \eta)$ is the efficiency of the leading leg of the appropriate double trigger, and $\varepsilon_{\mathrm{D,trailing}}(p_T,\, \eta)$ is the efficiency of the trailing leg of the appropriate double trigger.

$$
\begin{aligned}
\varepsilon_{\ell\ell'}(p_T,\, \eta,\, p'_T,\, \eta') \quad = \quad & 1 - [(1 - \varepsilon_{\mathrm{D,leading}}(p_T,\, \eta))(1 - \varepsilon_{\mathrm{D,leading}}(p'_T,\, \eta')) && (12) \\
& + \varepsilon_{\mathrm{D,leading}}(p_T,\, \eta)(1 - \varepsilon_{\mathrm{D,trailing}}(p'_T,\, \eta')) && (13) \\
& + \varepsilon_{\mathrm{D,leading}}(p'_T,\, \eta')(1 - \varepsilon_{\mathrm{D,trailing}}(p_T,\, \eta))] && (14) \\
& + \varepsilon_S(p'_T,\, \eta')(1 - \varepsilon_{\mathrm{D,trailing}}(p_T,\, \eta)) \\
& + \varepsilon_S(p_T,\, \eta)(1 - \varepsilon_{\mathrm{D,trailing}}(p'_T,\, \eta')) && (15)
\end{aligned}
$$

The procedure of Equation 12 is applied to simulated Higgs boson decays to obtain an event-by-event weight factor. We find a trigger efficiency with respect to the offline selection of 98% for a Higgs boson mass of 115 GeV/c^2 and this increases with larger mass hypotheses to higher than 99% for masses above 160 GeV/c^2.

5.2 Jet Veto Efficiency

We apply a data-driven method to estimate the jet veto efficiency and its systematic uncertainties in data. In this method, the jet veto efficiency on W$^+$W$^-$ events in data $\epsilon_{\mathrm{W^+W^-}}$ is estimated to be the value obtained from simulation multiplied by a data to simulation scale factor from $Z/\gamma^* \to \ell\ell$ events such that,

$$\epsilon_{H\to \mathrm{W^+W^-}} = \epsilon_{\mathrm{Z}}^{data} (\frac{\epsilon_{\mathrm{W^+W^-}}}{\epsilon_{\mathrm{Z}}})^{MC}.$$

The uncertainty in $\epsilon_{\mathrm{W^+W^-}}$ can be factorized into the Z efficiency uncertainty in data and the $H \to$ W$^+$W$^-$/Z efficiency ratio uncertainty in simulation. The former is dominated by the statistical uncertainty, while theoretical uncertainties due to higher order corrections contribute most to the W$^+$W$^-$/Z efficiency ratio uncertainties.

The data to simulation correction factor is close to unity for the zero-jet and 1-jet bins, while we observe some disagreement for events with at least two reconstructd jets.

6 Systematic Uncertainties

Table 4 to be updated with correct values!

Table 4: Summary of all systematic uncertainties (relative).

Source	$qq \rightarrow$ $\mathrm{W^+W^-}$	$gg \rightarrow$ $\mathrm{W^+W^-}$	non-Z resonant VV	top	DY	$\mathrm{W+jets}$	$V(W/Z)+\gamma$
Luminosity	—	—	4.5	—	—	—	4.5
Trigger efficiencies	1.5	1.5	1.5	—	—	—	1.5
Muon efficiency	1.5	1.5	1.5	—	—	—	1.5
Electron id efficiency	2.5	2.5	2.5	—	—	—	2.5
Momentum scale	1.5	1.5	1.5	—	—	—	1.5
$E_{\mathrm{T}}^{\mathrm{miss}}$ resolution	2.0	2.0	2.0	2.0	3.0	—	1.0
Jet counting	—	5.4	5.4	—	—	—	5.4
Higgs cross section	—	—	—	—	—	—	—
WZ/ZZ cross section	—	—	3.0	—	—	—	—
$qq \rightarrow WW$ norm.	10	—	—	—	—	—	—
$gg \rightarrow WW$ norm.	—	50	—	—	—	—	—
$\mathrm{W+jets}$ norm.	—	—	—	—	—	36	—
top norm.	—	—	—	15	—	—	—
$Z/\gamma^* \rightarrow \ell\ell$ norm.	—	—	—	—	50	—	—
WZ/ZZ cross section	—	—	3.0	—	—	—	—
$W+\gamma$ cross section	—	—	3.0	—	—	—	30
Monte Carlo statistics	1	1	4	6	20	20	10

7 Cross Section Measurement

	data	all bkg.	$qq \to \mathrm{W}^+\mathrm{W}^-$	$gg \to \mathrm{W}^+\mathrm{W}^-$	$\mathrm{t\bar{t}} + tW$	W + jets
$ee + \mu\mu$	462	191.81 ± 9.11	283.52 ± 4.18	16.90 ± 0.59	46.71 ± 2.34	16.50 ± 3.93
$e\mu + \mu e$	668	303.24 ± 6.74	455.89 ± 3.28	26.98 ± 0.46	82.86 ± 1.87	43.01 ± 3.20
Total	1130	495.05 ± 9.11	739.40 ± 4.18	43.87 ± 0.59	129.57 ± 2.34	59.50 ± 3.93

	WZ/ZZ not included in the $Z/\gamma^* \to \ell\ell$	$Z/\gamma^* \to \ell\ell + WZ + ZZ$	$W + \gamma$	$Z/\gamma^* \to \tau\tau$
$ee + \mu\mu$	5.05 ± 0.15	22.44 ± 3.11	5.21 ± 1.36	0.00 ± 0.00
$e\mu + \mu e$	9.72 ± 0.20	1.01 ± 0.24	14.30 ± 2.97	0.73 ± 0.22
Total	14.77 ± 0.25	23.45 ± 3.12	19.51 ± 3.26	0.73 ± 0.22

Table 5: Expected number of signal and background events from the data-driven methods for an integrated luminosity of 4.63 fb^{-1}after applying the selection requirements. Statistical uncertainties only.

variable	value	uncertainty
N_{data}	xxx	—
N_{bkg}	xxx	yyy
ϵ (%)	xxx	yyy
4.63 fb^{-1} (pb)	xxx	yyy
$BR(W \to \ell\nu)$	0.1080	0.0009

Table 6: Summary of the pieces to compute the WW cross-section and its uncertainty.

All pieces to compute the WW cross-section and its uncertainty are listed in Tab. 6. In summary, we obtain the following WW cross-section measurement using eq. **??**:

$$\sigma_{WW \to 2\ell 2\nu} = xxx \pm aaa\ (stat.) \pm bbb\ (syst.) \pm ccc\ (lumi.)\ pb,$$

or using the well-known $W \to l\nu$ branching ratio, we obtain:

$$\sigma_{WW} = xxx \pm aaa\ (stat.) \pm bbb\ (syst.) \pm ccc\ (lumi.)\ pb$$

The systematic uncertainty has two components: efficiency and background, while the luminosity is a separate term. We also compute the WW to W cross-section ratio, in which the luminosity uncertainty cancels out. The uncertainty contributions for the signal efficiency and background contamination can be considered mostly uncorrelated since the correlated factors are just a very small fraction of the overall uncertainty. We take the $W \to \ell\nu$ cross-section from [**?**], and hence obtain the following cross-section ratio:

$$\frac{\sigma_{WW}}{\sigma_W} = (xxx \pm aaa \pm bbb) \cdot 10^{-4},$$

in agreement with the expected theoretical ratio $(4.45 \pm 0.30) \cdot 10^{-4}$ from (N)NLO computations [**?**, **?**, **?**].

8 Anomalous Couplings

9 Summary

References

[1] K. Nakamura et al. (Particle Data Group), "Review of particle physics", J. Phys.G37 , 2010.

[2] F. Englert and R. Brout, "Broken symmetries and the masses of gauge bosons", Phys. Rev. Lett. 13, 1964.

[3] P. W. Higgs, "Broken symmetry and the mass of gauge vector mesons", Phys. Rev. Lett. 13, 1964.

[4] Guralnik, G.S. and Hagen, C.R. and Kibble, T.W.B., "Global Conservation Laws and Massless Particles", Phys.Rev.Lett. 13, 1964.

[5] M. Dittmar and H. K. Dreiner, Phys. Rev. D **55** (1997) 167".

[6] CMS Collaboration, "Measurement of WW Production and Search for the Higgs Boson in pp Collisions at $\sqrt{s} = 7$ TeV", arXiv:1102.5429.

[7] W. Andrews, et al., A Higgs Boson Search in the Fully Leptonic W^+W^- Final State, CMS AN-2011/155 (2011).

[8] W. Andrews, et al., A Higgs Boson Search in the Fully Leptonic W^+W^- Final State with the Full 2011 Dataset, CMS AN-2011/456 (2011).

[9] F. Stoeckli, "http://indico.cern.ch/getFile.py/access?contribId=0&resId=1&materialId=slides&confId=49009", EWK Diboson meeting of March 12 2009.

[10] /afs/cern.ch/cms/CAF/CMSCOMM/COMM_DQM/certification/Collisions11/7TeV/Prompt/Cert_160404-163869_7TeV_PromptReco_Collisions11_JSON.txt.

[11] A. Vartak, M. LeBourgeois, V. Sharma, "Lepton Isolation in the CMS Tracker, ECAL and HCAL", CMS AN-2010/106.

[12] S. Xie, *et al.*, "Electron Identification Using Multivariate Methods", CMS AN-2011/413.

[13] W. Erdmann, M. LeBourgeois, B. Mangano, https://indico.cern.ch/getFile.py/access?contribId=5&sessionId=3&resId=1 note in preparation.

[14] B. Mangano *et al.*, "Improvement in Photon Conversion Rejection Performance Using Advanced Tracking Tools", AN-10-283.

[15] S. Xie, *et al.*", "Study of Data-Driven Methods for Estimation of Fake Lepton Backgrounds", CMS AN-2009/120.

[16] W. Andrews, *et al.*, "Fake Rates for dilepton Analyses", CMS AN-2010/257.

[17] F. Golf, D. Evans, J. Mulmenstadt *et al.*, "Expectations for observation of top quark pair production in the dilepton final state with the early CMS data", CMS AN-2009/050.

[18] W. Andrews, et al., A Method to Measure the Contribution of $Z/\gamma^* \to \ell\ell$ to a di-lepton+ MET Selection, CMS AN-2009/023 (2009).

[19] CMS Collaboration, "Jet Energy Calibration with Photon+Jet Events", PAS JME-09-004.

[20] CMS Collaboration, "Jet Performance in pp Collisions at $\sqrt{s} = 7$ TeV", PAS JME-10-003.

[21] CMS collaboration, "Commissioning of b-jet identification with pp collisions at $\sqrt{s} = 7$ TeV, BTV-10-001.

[22] Cacciari, Matteo and Salam, Gavin P. and Soyez, Gregory, "The anti-k_t jet clustering algorithm", JHEP 04, 2008.

[23] W. Andrews, *et al.*, "Study of photon conversion rejection at CMS", CMS AN-2009/159.

[24] A. Hoecker, *et al.*, "TMVA - Toolkit for Multivariate Data Analysis", arXiv:physics/0703039, 2007.

[25] CMS Generator group, Standard Model Cross Sections for CMS at 7 TeV, 2010.

[26] PDF4LHC Working Group, `http://www.hep.ucl.ac.uk/pdf4lhc/PDF4LHCrecom.pdf`.

[27] Nadolsky, Pavel M. and others, "Implications of CTEQ global analysis for collider observables", Phys. Rev. D78 2008.

[28] Martin, A. D. and Stirling, W. J. and Thorne, R. S. and Watt, G., "Parton distributions for the LHC, Eur. Phys. J. C63 2009.

[29] Ball, Richard D. and others, "A first unbiased global NLO determination of parton distributions and their uncertainties", arXiv 1002.4407.

[30] A. O'Hagan and J.J. Forster, "Bayesian Inference", Kendall's Advanced Theory of Statistics, Arnold, London, 2B, 2004.

[31] G. Bauer *et. al.*, "Lepton ef?iencies for the inclusive W cross section measurement with 36.1pb^{-1}", AN2011/097.

[32] W. Andrews *et. al.*, "Uncertainties on the Lepton Selection Efficiency for $t t\bar{t}$ Cross Section Analysis", AN2010/274.

[33] David Sabes, "Electron reconstruction efficiency", https://indico.cern.ch/getFile.py/access?contribId=2&resId=0&materialId=slides&confId=140397.

[34] LHC Higgs Cross Section Working Group, "Handbook of LHC Higgs Cross Sections: Inclusive Observables", CERN-2011-002, 2011.

[35] CMS Collaboration, "CMS MET Performance in Events Containing Electroweak Bosons from pp Collisions at $\sqrt{s} = 7$ TeV", CMS PAS JME-2010-005 (2010).

[36] M. Zanetti, "MET with PU in $H \to W^+W^- \to 2\ell 2\nu$", https://indico.cern.ch/conferenceDisplay.py?confId=131580; B. Hooberman, "MET with PU in MC and First 2011 Data", https://indico.cern.ch/contributionDisplay.py?contribId=5&confId=132579.

[37] Mingshui Chen and Andrey Korytov, https://mschen.web.cern.ch/mschen/lands/.

[38] J. Campbell, R.K. Ellis, G. Zanderighi, "Next-to-Leading order Higgs + 2 jet production via gluon fusion.", JHEP 0610:028 (2006), hep-ph/0608194.

[39] J. Campbell, R.K. Ellis, C. Williams, "Vector boson pair production at the LHC.", arxiv:hep-ph/1105.0020.

[40] M. Plummer, "Jet Another Gibbs Sampler", http://www-ice.iarc.fr/m̃artyn/software/jags/.

[41] W. Andrews *et. al.*, "Shape analysis for Higgs searches in di-lepton final state", CMS AN2011/408.

[42] J. Campell, F. Tramontano, "Next-to-leading order corrections to Wt production and decay", arxiv:hep-ph/0506289.

[43] C.D. White, S. Frixione, E. Leanen, F. Maltoni *et. al.*, "Isolating Wt production at the LHC", arxiv:hep-ph/0908.0631.

[44] R. C. Gray, C. Kilic, M. Park, S. Somalwar and S. Thomas, "Backgrounds To Higgs Boson Searches from Asymmetric Internal Conversion", arXiv:1110.1368 [hep-ph].

[45] T. Junk, "Confidence level computation for combining searches with small statistics", Nucl.Instrum.Meth. **A434** (1999) 435443, arXiv:hep-ex/9902006. doi:10.1016/S0168-9002(99)00498-2.

[46] A. L. Read, "Modified frequentist analysis of search results (the CLs method)", CERN Yellow Report CERN-2000-005 (2000) 81.

[47] ATLAS Collaboration, CMS Collaboration, and LHC Higgs Combination Group, "Procedure for the LHC Higgs boson search combination in summer 2011", (July, 2011)